A visco-hypoplastic model for normally consolidated and overconsolidated clays

Yu-Qi He[a], Zhen-Yu Yin[a,*], Shun Wang[b,c]

[a]*Department of Civil and Environmental Engineering, The Hong Kong Polytechnic University, Kowloon, Hong Kong 999077, China*

[b]*State Key Laboratory of Water Resources Engineering and Management, Wuhan University, Wuhan 430072, China*

[c]*Institute of Engineering Risk and Disaster Prevention, School of Water Resources and Hydropower Engineering, Wuhan University, Wuhan 430072, China*

Abstract

This paper develops a new time-dependent hypoplastic model for normally consolidated and overconsolidated clays. A novel viscous strain rate formulation is derived from the isotach concept and incorporated into the total strain rate of the hypoplastic framework, allowing for viscous deformation at the onset of loading. The hypoplastic flow rule is defined for the direction of the viscous strain rate and its intensity directly linked to the overconsolidation ratio (OCR) and secondary compression coefficient. The Matsuoka-Nakai criterion is further introduced into the strength parameter through the transformed stress technique, enabling the model to describe the stress-strain-time behaviour of clays in general stress space. In addition, a new scalar function is proposed and implemented into the model to consider the OCR effect on the initial stiffness. The model predictive ability is finally examined by simulating laboratory tests on three different clays with various OCRs and stress paths, demonstrating that the model can capture the rate dependency, stress relaxation, and creep behaviours for both normally consolidated and overconsolidated clays under various loading conditions.

Keywords: Clays, Hypoplastic model, Rate dependency, Stress relaxation, Creep

*Corresponding author. Email: zhenyu.yin@polyu.edu.hk

1. Introduction

Time-dependent behaviours of clays are often observed in geotechnical investigations, encompassing phenomena such as strain rate dependency, stress relaxation, and creep upon loading (Lai et al., 2014; Acikel et al., 2018; Bagheri et al., 2019; Wang et al., 2024). Over the past few decades, numerous experimental and numerical studies have been conducted to study the time-dependent behaviour of clays (Karstunen and Yin, 2010; Yin et al., 2017), and remarkable achievements have been made. In engineering practices, many geostructures like embankments, retaining walls, and slopes are sensitive to the time-dependent behaviour of clays (Bjerrum, 1967). Therefore, reliable predictions of the time-dependent behaviour of clays and the long-term performance of constructions are of great significance. Developing a simple and suitable time-dependent constitutive model for clays remains challenging.

The most prevalent time-dependent constitutive models for clays are elastoviscoplastic (EVP) models that developed within the framework of elastoplasticity (Yin and Graham, 1999; Yin et al., 2002; Karim and Gnanendran, 2014). Among them, the overstress theory (Perzyna, 1963) and isotach concept (Šuklje, 1957) are frequently used. The overstress EVP model introduces a viscous scalar multiplier to represent the viscous strain increment, which depends on the distance between the static yield surface and the current loading surface. Early overstress EVP models (Adachi and Oka, 1982) employed the yield function of the cam-clay model to describe the static yield surface and the current loading surface. As a result, these models can not describe the tertiary creep and the time-dependent behaviour of heavily overconsolidated clays (Yao et al., 2015). To remedy this, Yin et al. (2002) proposed a new creep function and redefined the current loading surface, enabling those EVP models to encompass heavily overconsolidated clays. In addition, some approaches assume that no purely elastic region exists in

clays and use a mapping rule to calculate the viscoplastic strain under an arbitrary state (Kutter and Sathialingam, 1992). The isotach concept was first introduced by Šuklje (1957), where clay compressibility relies on the viscoplastic strain rate. Leroueil et al. (1985) later refined this concept and suggested a unique relationship between the viscoplastic strain rate and the current stress level in both one-dimensional and isotropic compression tests. Many isotach EVP models have since been developed (Freitas et al., 2011; Cheng and Yin, 2024; Wang and Cui, 2024; Zhao et al., 2024), clearly describing the stress-strain-time relationship of clays under various loading conditions. Despite these advancements, isotach models face challenges in accurately predicting creep and stress relaxation behaviours of heavily overconsolidated clays (Yang et al., 2016). In addition, as pointed out by Yuan and Whittle (2021), isotach models with the stress state and void ratio from laboratory tests notably overestimate the creep rate of normally consolidated clays under field conditions.

As an alternative to the prevailing EVP models, the hypoplastic constitutive model has rapidly developed over the past thirty years (Liao and Yang, 2021; Qian et al., 2023, 2024; Liao et al., 2024; Wang and Wu, 2024; Zhu et al., 2024). Its primary advantage involves avoiding decomposing strains into elastic and plastic parts, resulting in extremely simple formulations (Wu et al., 2017). The hypoplastic model was initially conceived for sand (Wu and Bauer, 1994) and subsequently developed for clays (Wang and Wu, 2021). Some salient features of natural clays, including inherent anisotropy, overconsolidation, and structure degradation, can be well predicted by the recently proposed hypoplastic models (Mašín, 2007; He et al., 2022, 2023). However, when it comes to modelling the time-dependent behaviour of clays, the hypoplastic approach appears to encounter challenges. In general, two approaches are employed within hypoplasticity to describe the time-dependent behaviour of soils. The first method involves dividing the stress tensor into inviscid and viscous parts, such as the models proposed by Xu et al.

(2016) and Wang et al. (2018). These models require an accelerated strain rate to simulate the viscous behaviour, allowing them to successfully capture the primary, secondary, and tertiary creep of soils. However, the incorporation of the accelerated strain rate makes the hypoplastic framework more complex, limiting its numerical applications. The second approach aims to decompose the strain rate into elastic and viscous parts, known as the visco-hypoplastic (VHP) model (Niemunis, 2003; Gudehus, 2004). The foundational framework of the VHP model was first proposed by Niemunis (2003), assuming that the viscous strain rate is a function of the Cauchy stress tensor and the void ratio. Upon loading, the viscous strain rate aligns with the direction of the hypoplastic flow rule. The basic VHP model can reproduce the time-dependent behaviour of normally and slightly overconsolidated clays, including rate dependency, stress relaxation, and the primary and secondary creep phases of clays (Fuentes et al., 2018). Nevertheless, it faces challenges in accurately predicting the tertiary creep phase of clays. In addition, the viscous strain rate in the VHP model is controlled by a reference strain rate, which is empirically given rather than experimentally determined. Recent advances have also incorporated strength anisotropy and structure effects (Fuentes and Lizcano, 2010) into the VHP model. For instance, Niemunis et al. (2009) introduced an anisotropic preconsolidation surface to describe anisotropic behaviours, while Jerman and Mašín (2020) rotated the asymptotic state boundary surface to an anisotropic shape using a second-order symmetric tensor. Despite these enhancements, further refinement is essential in refining the foundational assumption concerning the viscous strain rate within the VHP model.

This paper develops a new time-dependent hypoplastic model for clays based on the general VHP framework proposed by Niemunis (2003). A novel viscous strain rate is first mathematically derived from the isotach concept and employed in the hypoplastic framework to account for viscous behaviours. Compared to the viscous strain rate proposed by Niemunis (2003), the

newly proposed one shows enhanced physical significance while maintaining simplicity. Moreover, a transformed stress technique is used to incorporate the Matsuoka-Nakai failure criterion (Matsuoka, 1974) into the proposed model. As a result, the stress-strain-time relationship of clays can be predicted under multiaxial conditions. Additionally, a stiffness function is included in the proposed model to consider the effect of overconsolidation on the initial stiffness. The proposed model requires nine parameters, including five basic parameters, two viscous parameters, and two additional parameters. It can reasonably describe the rate dependency, stress relaxation, and creep behaviours of normally consolidated and overconsolidated clays under different loading conditions.

2. Basic hypoplastic equations

In this paper, second-order tensors are denoted with bold letters (e.g., $\mathbf{T}$, $\mathbf{D}$) and fourth-order tensors with calligraphic bold letters (e.g., $\boldsymbol{\mathcal{L}}$). The tensor operations are: $\mathbf{A}\cdot\mathbf{B} = A_{ik}B_{kj}$, $\mathbf{A}{:}\mathbf{B} = A_{ij}B_{ij}$, $\mathbf{A}\otimes\mathbf{B} = A_{ij}B_{kl}$, and $\boldsymbol{\mathcal{L}}{:}\mathbf{D} = \mathcal{L}_{ijkl}A_{kl}$. The quantity $\|\mathbf{A}\| = \sqrt{\mathbf{A}{:}\mathbf{A}}$ denotes the Euclidean norm of $\mathbf{A}$. $\mathrm{tr}\mathbf{A} = \mathbf{A}_{ii}$ refers the trace of $\mathbf{A}$, and $\mathbf{A}^* = \mathbf{A}\text{-}\mathbf{I}(\mathrm{tr}\mathbf{A})/3$ signifies the deviatoric part of $\mathbf{A}$. The unit tensors of the second and fourth orders are $\mathbf{I}$ ($I_{ij} = \delta_{ij}$) and $\boldsymbol{\mathcal{I}}$ ($I_{ijkl} = 1/2(\delta_{ik}\delta_{jl} + \delta_{il}\delta_{jk})$), respectively.

2.1. General framework

Let us first consider the following general framework for the visco-hypoplastic model proposed by Niemunis (2003):

$$\mathring{\mathbf{T}} = \boldsymbol{\mathcal{L}}{:}(\mathbf{D} - \mathbf{D}_{vis}) \tag{1}$$

where $\boldsymbol{\mathcal{L}}$ represents a fourth-order tensor analogous to the elastic stiffness matrix. $\mathbf{D}$ and $\mathbf{D}_{vis}$ refer to the strain rate and viscous strain rate tensors, respectively. $\mathbf{D}_{vis}$ is a function of the Cauchy stress tensor and the void ratio:

$$\mathbf{D}_{vis} = D_r(\frac{1}{\mathrm{OCR}})^{-1/I_v}\mathbf{B} \tag{2}$$

where D_r and I_v denote the reference creep rate and viscosity index, respectively. OCR means the overconsolidation ratio. The second-order tensor $\mathbf{B}$ denotes the flow rule of the hypoplastic model (Wu and Kolymbas, 2000), defined as

$$\mathbf{B} = \frac{\mathbf{D}}{\|\mathbf{D}\|} = -\boldsymbol{\mathcal{L}}^{-1}\mathbf{:N} \tag{3}$$

where $\mathbf{N}$ is a second-order tensor function representing the nonlinear term of the hypoplastic model.

The Jaumann stress rate $\mathring{\mathbf{T}}$ is defined as

$$\mathring{\mathbf{T}} = \dot{\mathbf{T}} + \mathbf{TW} - \mathbf{WT} \tag{4}$$

where $\mathbf{T}$ and $\dot{\mathbf{T}}$ are the Cauchy stress tensor and its time derivative, respectively. $\mathbf{W}$ is the spin tensor.

The strain rate and spin tensors are

$$\mathbf{D} = [\nabla\mathbf{v} + (\nabla\mathbf{v})^{\mathsf{T}}]/2, \qquad \mathbf{W} = [\nabla\mathbf{v} - (\nabla\mathbf{v})^{\mathsf{T}}]/2 \tag{5}$$

where $\mathbf{v}$ denotes the velocity. ∇ and T are gradient and transposition operators, respectively.

2.2. Reference model

To describe the mechanical behaviour of overconsolidated clays, Wang and Wu (2021) proposed the following hypoplastic model:

$$\mathring{\mathbf{T}} = f_s\Big[(\mathrm{tr}\check{\mathbf{T}})\mathbf{D} + f_v(\mathrm{tr}\mathbf{D})\check{\mathbf{T}} + a^2\frac{\mathrm{tr}(\check{\mathbf{T}}\mathbf{D})}{\mathrm{tr}\check{\mathbf{T}}}\check{\mathbf{T}} + af_u(\hat{\mathbf{T}} + \hat{\mathbf{T}}^*)\|\mathbf{D}\|\Big] \tag{6}$$

where $\check{\mathbf{T}} = \mathbf{T}+\mathbf{S}$ and $\hat{\mathbf{T}} = \mathbf{T}-\mathbf{S}$ are adopted for simplicity. $\mathbf{S}$ is a structure tensor representing the overconsolidation:

$$\mathbf{S} = \alpha\ln(\frac{1}{R})\mathbf{T} \tag{7}$$

where α is a model parameter, and $R = 1/\mathrm{OCR}$ is a stress ratio indicating the degree of overconsolidation. The multipliers f_s and f_v are state-dependent functions that control the initial stiffness and the volumetric variation of the model, respectively. Which can be expressed as

$$f_s = -\frac{2}{3v_i\lambda}, \qquad f_v = \frac{3}{2}v_i - \frac{1}{3}(3 + a^2 - \sqrt{3}a) \tag{8}$$

in which v_i and λ are model parameters. The strength parameter a can be obtained through

$$a = \frac{\sqrt{3}(3 - \sin\varphi)}{2\sqrt{2}\sin\varphi} \tag{9}$$

where φ is the critical friction angle.

The multiplier f_u is used to improve the undrained stress path prediction, defined as

$$f_u = \frac{|\mathbf{B}{:}\mathbf{D}|}{\|\mathbf{B}\|\ \|\mathbf{D}\|} \tag{10}$$

The above hypoplastic model requires only five parameters and can effectively capture the

mechanical behaviour of normally consolidated and overconsolidated clays under different loading conditions.

3. Visco-hypoplastic model

3.1. Viscous strain rate

Several VHP models (Niemunis et al., 2009; Fuentes and Lizcano, 2010; Fuentes et al., 2018) have been developed based on the viscous strain rate formulated in Eq. (2). These models offer advantages such as fewer model parameters and easy numerical implementation. However, the viscous strain rate in Eq. (2) was assumed empirically, and there is no basis for the determination of D_r. In this section, a novel viscous strain rate for hypoplasticity is proposed based on the isotach concept.

When considering the stress-strain-time behaviour of clays, it is commonly assumed that the time-dependent deformation of clays can be categorized into primary compression and secondary compression (Bjerrum, 1967). The former is induced by an instant volume strain, accompanied by the dissipation of excessive pore pressure. The secondary compression is caused by a delayed volume strain, involving the phenomenon of creep under constant effective pressure, as shown in Fig. 1.

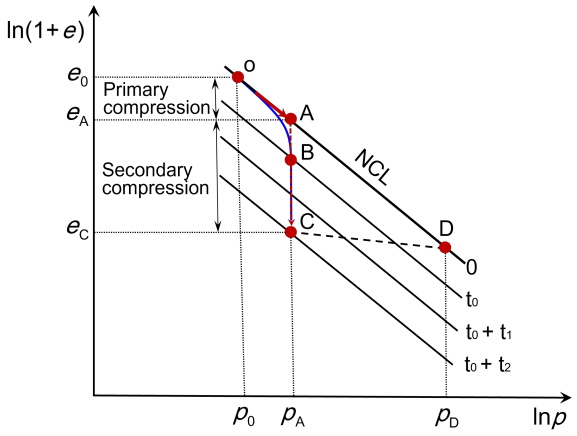

Figure 1: Isotropic compression lines of clays at different times.

Fig. 2 illustrates the compression behaviour of clays in the double logarithmic plane $\ln(1+e)$ – $\ln t$. It can be seen that the deformation stage before the inflection point B corresponds to the primary compression, followed by the secondary compression stage BC, which manifests as an almost linear trend and can be mathematically represented by a logarithmic function:

$$\ln(1+e) = e_i - C^*_{\alpha e}\ln(t/t_0) \tag{11}$$

in which e_i is the initial void ratio, $C^*_{\alpha e}$ represents the coefficient of secondary consolidation in the $\ln(1+e)$ – $\ln t$ plane, t denotes the creep time, and t_0 means the reference time. However, Eq. (11) can not consider the case when $t = 0$. According to Yao et al. (2015), an updated expression of Eq. (11) is given as

$$\ln(1+e) = e_i - \beta\ln(t/t_0 + 1) \tag{12}$$

where β is a new viscous parameter, representing the slope of the secondary compression line in the $\ln(1+e)$ – $\ln(t/t_0+1)$ plane. In this study, $t_0 = 1$ min is adopted for convenience (Yao et al., 2015).

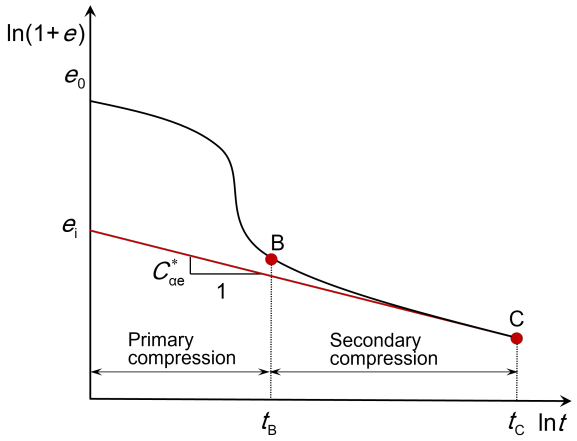

Figure 2: The compression behaviour of clays in the $\ln(1+e)$ – $\ln t$ plane.

Differentiating Eq. (12), the increment of the viscous volumetric strain $d\varepsilon_{vis}$ can be obtained:

$$d\varepsilon_{vis} = \beta \frac{dt}{t + t_0} \tag{13}$$

where dt is the increment of the real time. The viscous volumetric strain rate can consequently be determined as:

$$D_{vis} = \beta \frac{1}{t + t_0} \tag{14}$$

As shown in Fig. 1, the normal compression line (NCL) corresponds to the case $t_a = 0$. As a result, the variation in void ratio along the creep path AC can be expressed as

$$\Delta e|_{\mathrm{AC}} = -\beta \ln(t/t_0 + 1) \tag{15}$$

Furthermore, in the case of a normally consolidated clay, the current state point is located on the NCL, as shown in Fig. (1). In other words, the NCL can be regarded as a reference line to calculate the overconsolidation degree of clays. Based on this, the variation in void ratio along the loading-unloading path ADC can be expressed as

$$\Delta e|_{\mathrm{ADC}} = -(\lambda^* - \kappa^*) \ln(p_{\mathrm{D}}/p_{\mathrm{A}}) = -(\lambda^* - \kappa^*) \ln \mathrm{OCR} \tag{16}$$

where p_{D} and p_{A} represent the mean effective stresses at points D and C, respectively, i.e., the preconsolidation stress and the current effective stress at point C. λ^* and κ^* are slopes of the normal compression and the unloading lines in the $\ln(1 + e)$ – $\ln p$ plane, respectively.

In the hypoplastic framework, the overconsolidation ratio in general states (Niemunis, 2003;

Wang and Wu, 2021) can be defined as

$$\mathrm{OCR} = p_e / p_e^+ \tag{17}$$

in which the Hvorslev equivalent pressure p_e is given as follows:

$$p_e = \exp\Big[\frac{N - \ln(1+e)}{\lambda^*}\Big] \tag{18}$$

To define the preconsolidation pressure p_e^+, we use the following yield equation:

$$f = \frac{1}{n}\frac{q^{(n+1)}}{M^{(n+1)}p^n} + p - p_e^+ = 0 \tag{19}$$

Therefore, we can obtain:

$$p_e^+ = p\Big[1 + \frac{1}{n}\big(\frac{q}{Mp}\big)^{(n+1)}\Big] \tag{20}$$

where q and p are effective deviatoric stress and mean stress, respectively. M is defined as $M = 6\sin\varphi/(3 - \sin\varphi)$, representing the slope of the critical state line. n is a parameter controlling the shape of the yield surface. Note that when $n = 1$, the yield equation in Eq. (20) evolves into the modified cam-clay (MCC) yield equation. The effect of n on the model performance will be discussed in Section 4.1.

Moreover, the changes in void ratios $\Delta e|_{\mathrm{AC}}$ and $\Delta e|_{\mathrm{ADC}}$ are identical. As a result, we can obtain the following equation by combing Eqs. (15), (16), and (17):

$$t = t_0(R^{-\alpha} - 1) \tag{21}$$

where $\alpha = (\lambda^* - \kappa^*)/\beta$ and $R = 1/\mathrm{OCR}$.

Substituting Eq. (21) into Eq. (14), the volumetric strain rate becomes

$$D_{vis} = \beta \frac{R^{\alpha}}{t_0} \tag{22}$$

The hypoplastic flow rule $\mathbf{B}$ is adopted as the direction of the viscous strain. As a result, a new viscous strain rate tensor is defined as

$$\mathbf{D}_{vis}^{new} = \beta \frac{R^{\alpha}}{t_0} \mathbf{B} \tag{23}$$

3.2. Linear and nonlinear terms

According to Wu and Kolymbas (2000), the hypoplastic framework can be expressed by a linear term $\boldsymbol{\mathcal{L}}$ and a nonlinear term $\mathbf{N}$ as

$$\mathring{\mathbf{T}} = f_s \Big[\boldsymbol{\mathcal{L}} : \mathbf{D} + \mathbf{N} \|\mathbf{D}\| \Big] \tag{24}$$

Based on Eq. (24) and using the reference model formulated in Eq. (6), new terms for the time-dependent hypoplastic model can be expressed as

$$\boldsymbol{\mathcal{L}} = (\mathrm{tr}\mathbf{T})\boldsymbol{\mathcal{I}} + f_v \mathbf{T} \otimes \mathbf{I} + a^2 \frac{\mathbf{T} \otimes \mathbf{T}}{\mathrm{tr}\mathbf{T}} \tag{25a}$$

$$\mathbf{N} = f_u a (\mathbf{T} + \mathbf{T}^*) \tag{25b}$$

Note that the reference model considers the overconsolidation by introducing a structure tensor $\mathbf{S}$ into the Cauchy stress tensor $\mathbf{T}$ ($\check{\mathbf{T}} = \mathbf{T} + \mathbf{S}$). However, the overconsolidation in the viscous hypoplastic framework is considered via the viscous strain rate tensor $\mathbf{D}_{vis}^{new}$. Therefore, the structure tensor $\mathbf{S}$ should be removed from the Cauchy stress tensor, as shown in Eq. (25).

Substituting Eqs. (3), (23), and (25) into Eq. (1), a new time-dependent hypoplastic equation can be recast as

$$\mathring{\mathbf{T}} = f_s \boldsymbol{\mathcal{L}} : (\mathbf{D} - \mathbf{D}_{vis}^{new}) \tag{26}$$

The functions f_s, f_v, f_u, and the strength parameter a remain consistent with the reference model.

3.3. Initial stiffness

The developed time-dependent hypoplastic model formulated in Eq. (26) can effectively predict the initial stiffness and critical state for normally consolidated clays. However, when dealing with overconsolidated clays, particularly heavily overconsolidated ones, it has been found that the initial stiffness remains constant despite increasing OCR values, as illustrated in Fig. 3(a). This observation conflicts with experimental findings where the initial stiffness generally increases with increasing OCR values (Han et al., 2021). To remedy this shortcoming, further improvements are required.

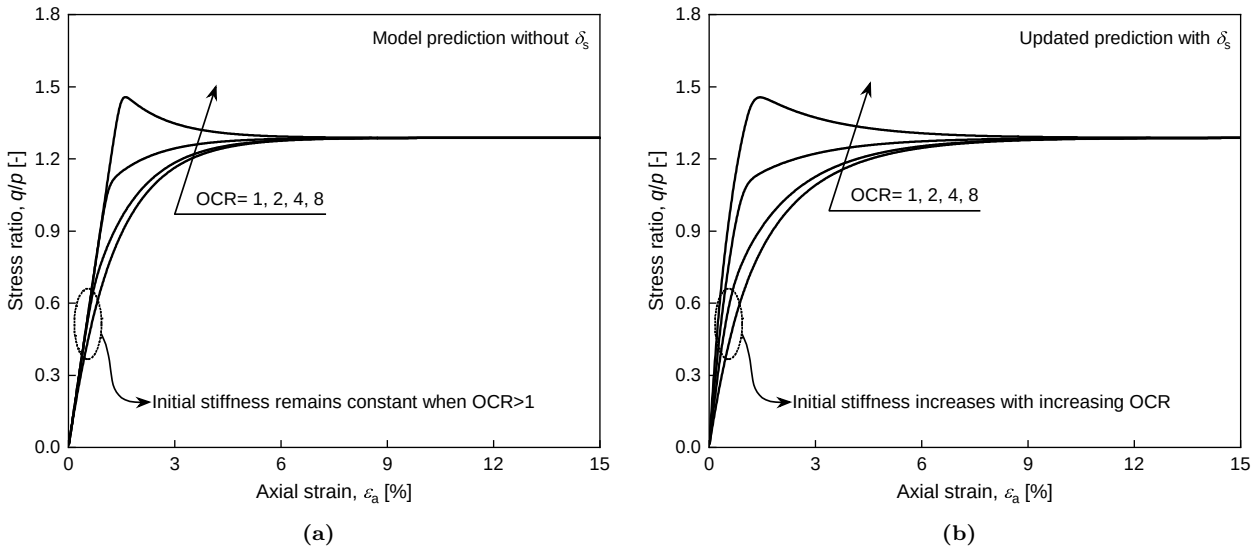

Figure 3: Model predictions for overconsolidated clays in undrained triaxial compression tests: (a) without δ_s; (b) with δ_s.

The hypoplastic framework presumes that the stress rate is a function of the stress and

strain rate. Based on this assumption, the initial stiffness of the model can be altered by multiplying a scalar factor on the entire hypoplastic model without changing the critical state, as the stress rate equals zero at the critical state. According to Wu and Kolymbas (2000), the following stiffness function considering OCR variation is proposed:

$$\delta_s = \frac{\exp[\zeta \ln(\mathrm{OCR})]}{(1 + r_s^2)} \tag{27}$$

where ζ is a material parameter controlling the initial stiffness of the overconsolidated sample. The stress ratio $r_s = \|\mathbf{T}^*\|/\mathrm{tr}\mathbf{T}$. Therefore, the stiffness function f_s becomes:

$$f_s = -\frac{2\delta_s}{3v_i\lambda^*} \tag{28}$$

Fig. 3(b) shows the updated predictions for clays with different OCRs in undrained compression tests. The result demonstrates that the initial stiffness varies with OCR values upon implementing the stiffness function δ_s, whereas the peak strength and critical state remain unchanged.

3.4. Failure surface

By making use of the definition of the norm $\|\mathbf{D}\|$ ($\mathbf{D}$:$\mathbf{D}/\|\mathbf{D}\|^2$=1), the failure surface of the proposed model can be revealed as

$$f(\mathbf{T}) = \mathbf{B}:\mathbf{B} - 1 = 0 \tag{29}$$

Substituting Eq. (3) into Eq. (29) yields the following explicit failure surface

$$f(\mathbf{T}) = \left(\mathbf{N}^{\mathsf{T}}:(\boldsymbol{\mathcal{L}}^{\mathsf{T}})^{-1}\right) : \left(\boldsymbol{\mathcal{L}}^{-1}:\mathbf{N}\right) - 1 = 0 \tag{30}$$

in which the superscript T denotes transposition.

However, the geometric shape of Eq. (30) on the π-plane is a circle (Fig. 4), indicating that the shear strength remains consistent under both triaxial compression and extension tests. This conflicts with the fact that the shear strength under triaxial compression conditions is typically greater than that under triaxial extension conditions. To remedy this, several attempts have been made to transform the conical failure surface of the reference hypoplastic model into a non-conical one, including the utilization of an interpolation function (Zhang et al., 2021) and transformed stress (TS) technique (He et al., 2023). In this paper, the TS method (Tian and Yao, 2017) is used to introduce the Matsuoka-Nakai criterion (Matsuoka et al., 1999) into the proposed time-dependent hypoplastic model.

According to Tian and Yao (2017), the TS method operates on the deviatoric stress by multiplying a scalar factor while keeping the mean effective stress constant. It is assumed that the original principal stress space $(T_1 - T_2 - T_3)$ aligns coaxially with the transformed principal stress space $(\widetilde{T}_1 - \widetilde{T}_2 - \widetilde{T}_3)$, and the stress states before and after transformation are as follows:

$$\tilde{p} = p, \qquad \tilde{q} = q, \qquad \tilde{\theta} = \theta \tag{31}$$

where p and q refer to the mean effective stress and deviatoric stress, respectively, θ denotes the Lode's angle, and the superscript $\tilde{}$ means the stress in the transformed stress space. A mapping rule from $\mathbf{T}$ to $\widetilde{\mathbf{T}}$ can be formulated as

$$\widetilde{\mathbf{T}} = \begin{cases} \dfrac{\mathrm{tr}\mathbf{T}}{3}\mathbf{I} + \dfrac{q_c}{q}\mathbf{T}^*, & (q \neq 0) \\ \mathbf{T}, & (q = 0) \end{cases} \tag{32}$$

where q_c means the deviatoric stress at the triaxial compression state on the π-plane. Based

on the Matsuoka-Nakai criterion, q_c can be expressed as

$$q_c = \frac{2I_1}{3\sqrt{(I_1 I_2 - I_3)/(I_1 I_2 - 9I_3)} - 1} \tag{33}$$

in which I_1, I_2, and I_3 are stress invariants. Note that q_c changes according to the failure criterion; one can refer to (Yao and Sun, 2000; Yao et al., 2004; Lu et al., 2017, 2019; Liang et al., 2019, 2022) for more failure criteria.

After transformation, the failure criterion of the original hypoplastic model can be updated to a non-linear one, i.e., the failure curve on the π-plane shifts from a circle to a curved triangle, as shown in Fig. 4. The complete formulation of the proposed constitutive model in Eq. (26) is given in the Appendix A. For further descriptions of the TS method, please refer to the Appendix B.

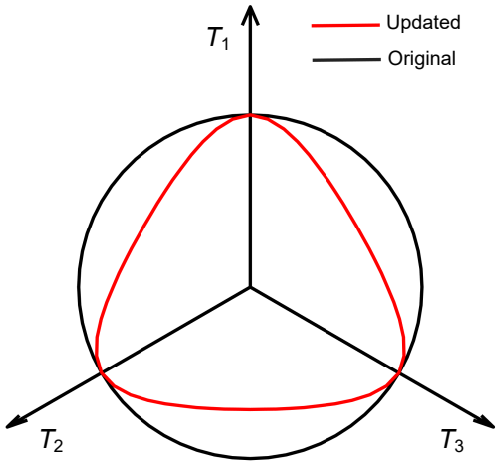

Figure 4: Original and updated failure curves on the π-plane.

Fig. 5 compares the results of undrained triaxial compression and extension tests as predicted by the proposed model with and without the TS method. The findings demonstrate that the updated model (with TS method) effectively captures the variation in shear strength between triaxial compression and extension tests. In simulations, the axial strain rate is maintained at

5%/h, and the viscous parameter β is specified as 0.003. The remaining parameters are listed in Table 1.

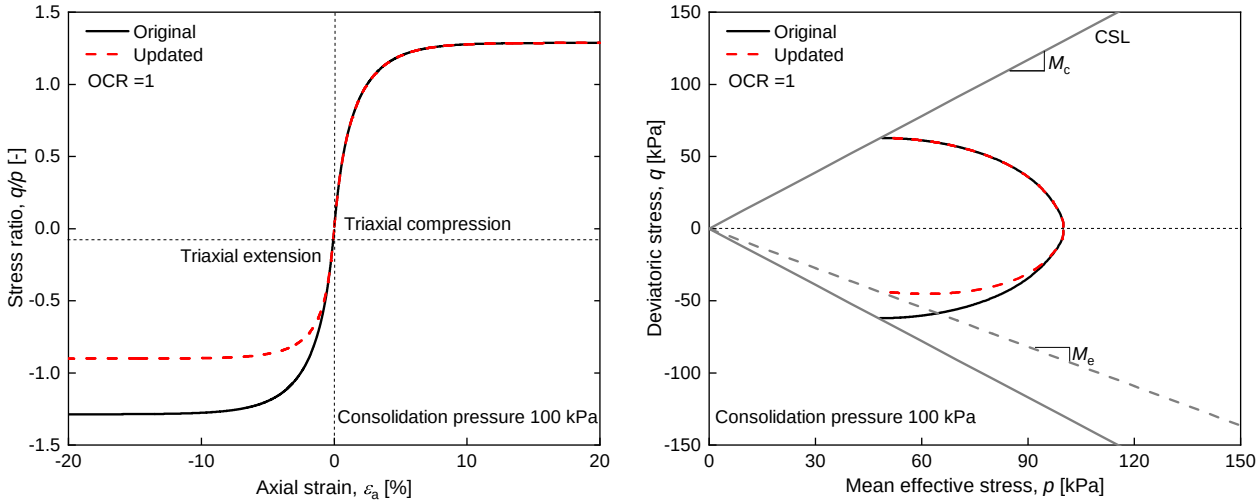

Figure 5: Original and updated model predictions in undrained triaxial compression and extension tests: (a) stress-strain curves; (b) stress paths.

4. Model parameters and discussions

In this section, we first summarize the model parameters and analyze their effects on model predictions. The uniqueness of the rate dependency is then investigated by simulating triaxial compression and oedometer tests using a single set of model parameters. Based on this, some illustrative simulations are conducted to evaluate the model performance when dealing with time-dependent effects, including rate dependency, stress relaxation, and creep behaviours.

4.1. Summary of model parameters

The proposed time-dependent hypoplastic model requires nine parameters, including five basic parameters: N, λ^*, κ^*, v_i, and φ, two viscous parameters: β and t_0, and two additional parameters: ζ and n. These parameters have the following physical meanings: N is the value of $\ln(1+e)$ at $p = 1$ kPa on the normal compression line of a reconstituted clay; λ^* is the slope of the normal compression line in the $\ln(1+e)$ – $\ln p$ plane; κ^* is the slope of the unloading line

in the $\ln(1+e)$ – $\ln p$ plane; v_i is the ratio of the bulk modulus in the isotropic compression test to the shear modulus in the undrained shear test; φ is the critical friction angle; β is the slope of the secondary compression curve in the $\ln(1+e)$ – $\ln(t/t_0+1)$ plane; t_0 is the reference time; ζ controls the initial stiffness of the model; n controls the critical state strength.

The parameters N, λ^*, and κ^* can be determined with an isotropic normal compression test. The parameters v_i and φ can be obtained through a conventional triaxial compression test. The parameter β can be determined by fitting the secondary compression curve in the $\ln(1+e)$ – $\ln(t/t_0+1)$ plane. The parameter t_0 is taken as $t_0 = 1$ min. The parameters ζ and n require curve fitting. The effect of the basic parameters on the proposed model is the same as those in the models proposed by Mašín (2005) and Wang and Wu (2021). Therefore, in the following, we mainly discuss the effect of the parameters β and n on the model performance through a series of undrained triaxial simulations. The numerical sample is normally and isotropically consolidated with a confining pressure of 400 kPa. Trial values of β and axial strain rates are used, while other parameters are listed in Table 1.

Table 1: Material parameters for model predictions

Parameters	N	λ^*	κ^*	v_i	$\varphi/^\circ$	ζ	n	t_0/min
Value	1.8	0.15	0.02	0.2	32	0.5	1	1

Fig. 6(a) illustrates undrained triaxial predictions of stress-strain curves with various β at a specified axial strain rate of $5\%/h$. The result shows that an increase in β will give rise to a decrease in the deviatoric stress. As a result, the stress path will slightly move downward under the same mean effective stress, as shown in Fig. 6(b).

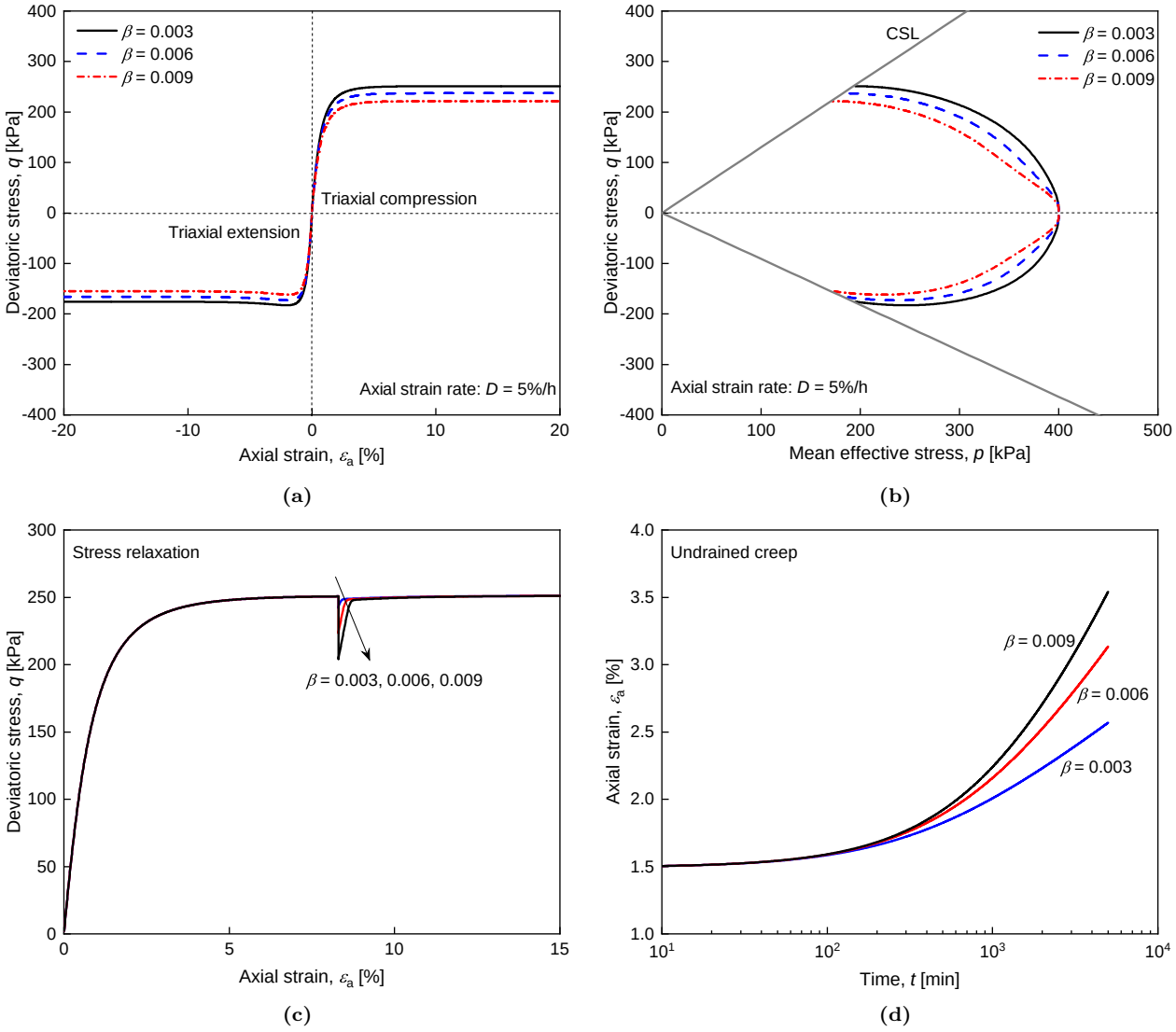

Figure 6: Model performance with different β in undrained tests: (a) stress-strain curves; (b) stress paths; (c) stress relaxation; (d) creep.

Furthermore, the proposed model can also describe the stress relaxation and creep behaviours of clays. Specifically, stress relaxation can be simulated by setting the strain rate to zero through $\mathring{\mathbf{T}} = f_s\boldsymbol{\mathcal{L}}\!:\!(\mathbf{0} - \mathbf{D}_{vis}^{new})$, while creep corresponds to $\mathbf{0} = f_s\boldsymbol{\mathcal{L}}\!:\!(\mathbf{0} - \mathbf{D}_{vis}^{new})$. Shown in Figs. 6(c) and (d) are the predicted stress relaxation and undrained creep behaviours. Obviously, with the increase of β, the stress relaxation and creep become more and more pronounced. The stress relaxation simulation begins at an axial strain of 8.3% with an initial constant strain rate of 5%/h. During the creep simulation, the creep load is controlled at 200 kPa.

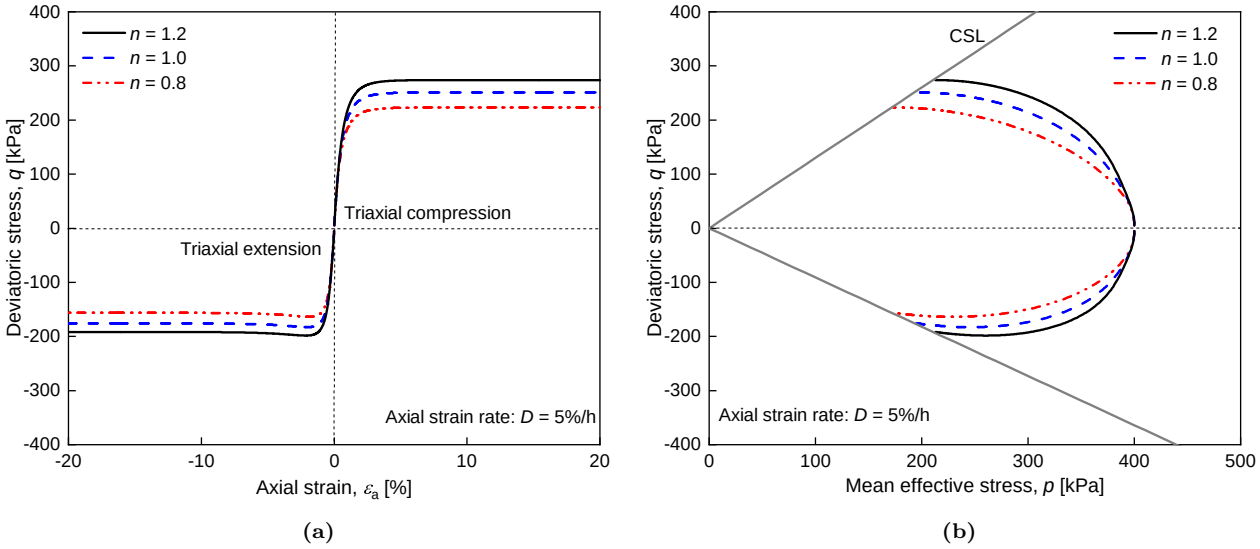

Figure 7: Model performance with different n in undrained triaxial compression and extension tests: (a) stress-strain curves; (b) stress paths.

Fig. 7 shows the effect of the parameter n on the model performance. It can be observed that n mainly controls the critical state strength of the model. Specifically, an increase in n will give rise to an increase in the critical state strength of the model in both triaxial compression and tension tests. This improvement substantially enhances the applicability of the model, enabling a better description of the strength characteristics of various clays.

It should be noted that the proposed viscous strain rate $\mathbf{D}_{vis}^{new}$ (Eq. (23)) is similar to the viscous strain rate $\mathbf{D}_{vis}$ proposed by Niemunis (2003) but with different physical meanings and parameter values. In Eq. (2), $\mathbf{D}_{vis}$ is given empirically and depends on the reference creep rate D_r and viscosity index I_v. Generally, D_r is taken as $10^{-6}/s$ and I_v ranges from 0.02 to 0.06 (Gudehus, 2004), which seriously limits the applicability of the model. In the proposed model, the viscous strain rate $\mathbf{D}_{vis}^{new}$ is derived from the isotach concept, with all parameters determined from experiments, resulting in a more theoretical expression.

4.2. Uniqueness of rate dependency

In this section, we aim to verify the uniqueness of rate dependency within the proposed model, i.e., to examine whether the rate effect in oedometer tests is the same as that in triaxial tests. According to Yin et al. (2011, 2015), under oedometric conditions, the relationship between the strain rate and the preconsolidation pressure in the double logarithmic plane can be defined as

$$\frac{D}{D^r} = \left(\frac{p_c}{p_c^r}\right)^{\alpha} \qquad \text{or} \qquad \frac{D_v}{D_v^r} = \left(\frac{p_c}{p_c^r}\right)^{\alpha} \tag{34}$$

where D and D^r denote the current and reference axial strain rates, respectively. D_v and D_v^r refer to the current and reference volumetric strain rates, respectively. p_c and p_c^r are the preconsolidation pressures corresponding to D(or D_v) and D_r(or D_v^r), respectively. α is a rate-dependent coefficient representing the slope of Eq. (34) in the double logarithmic plane.

Under undrained triaxial conditions, the relationship between the strain rate and the undrained peak strength in the double logarithmic plane can be defined as

$$\frac{D}{D^r} = \left(\frac{q_{peak}}{q_{peak}^r}\right)^{\alpha} \qquad \text{or} \qquad \frac{D_d}{D_d^r} = \left(\frac{q_{peak}}{q_{peak}^r}\right)^{\alpha} \tag{35}$$

where D_d and D_d^r are the current and reference deviatoric strain rates, respectively. q_{peak} and q_{peak}^r are the undrained peak strengths corresponding to D(or D_d) and D_r(or D_d^r), respectively.

In the present work, for oedometer and undrained triaxial tests, the preconsolidation pressure or undrained peak strength was normalized by its value at an axial strain rate of 0.5%/h. Then, these normalized values were plotted together versus the axial strain rate, as shown in Fig. 8. The result shows that there is a linear relationship between the normalized preconsolidaiton pressure (or undrained peak strength) and the axial strain rate, indicating a consistent rate effect under both undrained triaxial and oedometric conditions. That is, we can model

conventional triaxial and oedometer tests with a single set of parameters.

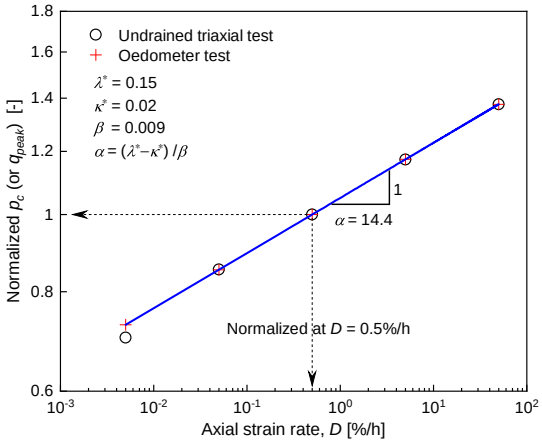

Figure 8: Normalized preconsolidation pressure and undrained peak strength versus axial strain rate.

Fig. 9 shows the predicted stress-strain curves and stress paths at different axial strain rates with $\beta = 0.003$ in undrained triaxial tests. The result demonstrates that a faster loading rate leads to a higher shear strength. In addition, the stress paths are also referred to as isotach, and their positions are determined by the strain rate.

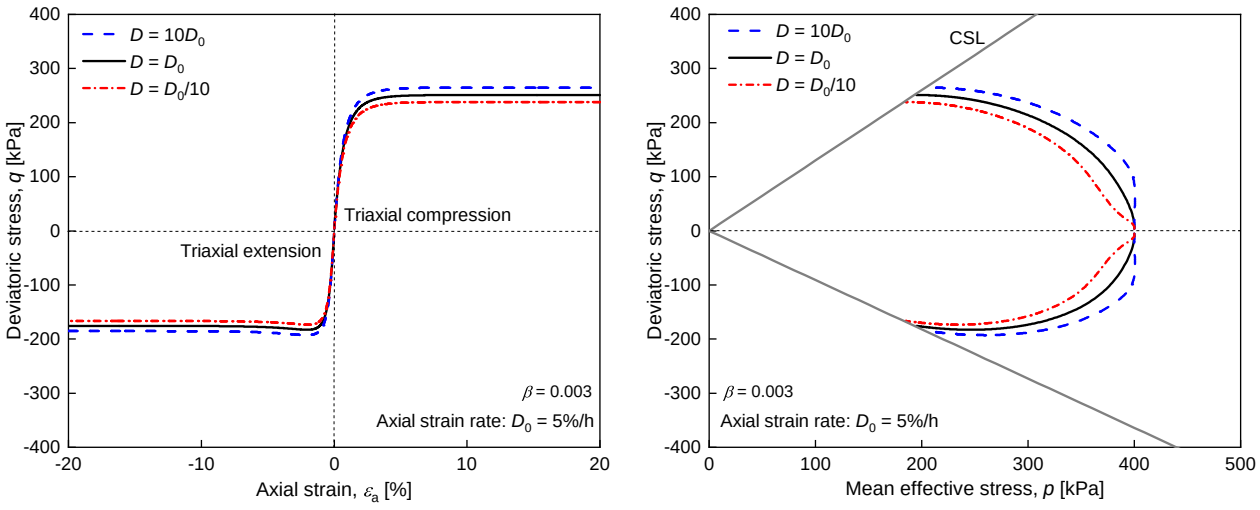

(a) **(b)**

Figure 9: Model performance with different axial strain rates in undrained triaxial compression and extension tests: (a) stress-strain curves; (b) stress paths.

Figs. 10(a) and (b) depict oedometer predictions of normal compression lines at different axial strain rates with $\beta = 0.003$ and $\beta = 0.03$, respectively. The result indicates that the

magnitude of the rate effect in the proposed model is governed by the parameter β; specifically, a greater β leads to a more pronounced rate effect.

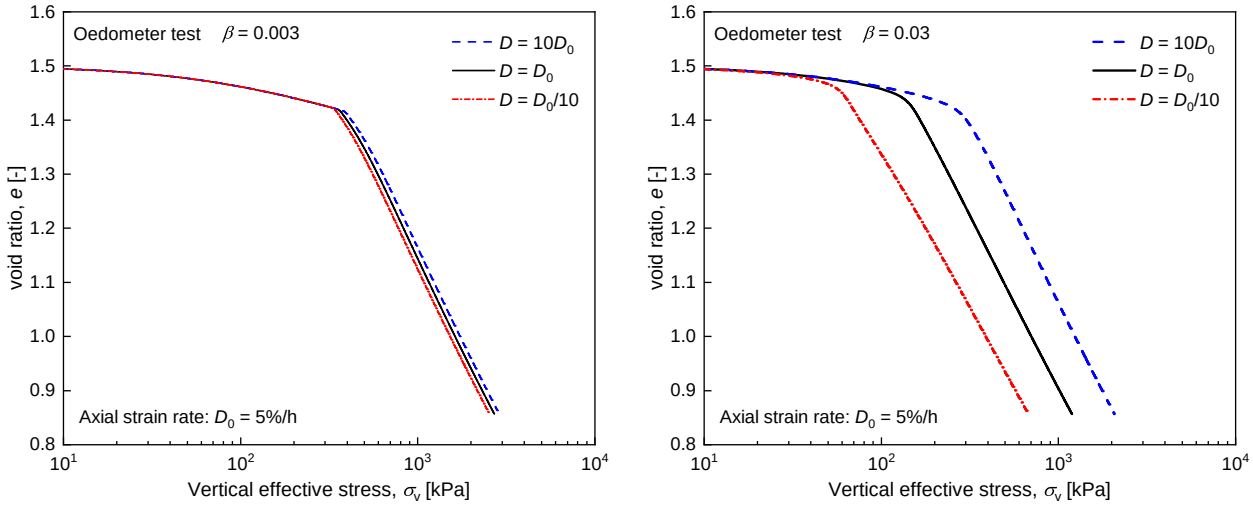

Figure 10: Model performance with different axial strain rates in oedometer tests: (a) $\beta = 0.003$; (b) $\beta = 0.03$.

5. Experimental validation

In this section, we will evaluate the proposed model by comparing model predictions to experimental results under different loading conditions. These tests can be divided into four groups, including constant strain rate tests on normally and overconsolidated Hong Kong marine deposits (HKMD) (Zhu, 2000), stage-changed strain rate tests on St. Herblain clay (Yin et al., 2010), stress relaxation tests on Estuarine clay (Kelln et al., 2008), and creep tests on HKMD. The simulation parameters are listed in Table 2, in which the parameters N, λ^*, κ^*, and φ are obtained from literature, while the parameters β, v_i, ζ, and n are determined through curving fitting to gain the best match with experimental results. Note that in this paper, the basic parameters N, λ^*, and κ^* are measured in the $\ln(1+e)$ – $\ln p$ plane, which is different from the generally used values in the e – $\ln p$ plane. The parameter ζ is only used for simulations of overconsolidated clays since Eq. (27) is a constant for normally consolidated clays (OCR = 1).

Table 2: Material parameters for model validation

Parameters	N	λ^*	κ^*	v_i	$\varphi/^\circ$	β	ζ	n	t_0/min
Hong Kong marine deposits	1.2	0.12	0.015	0.2	31.6	0.003	0.5	1.3	red1
St.Herblain clay	1.8	0.15	0.007	0.2	31.1	0.008	0.5	1.2	1
Estuarine clay	1.5	0.09	0.02	0.5	29.1	0.002	0.8	1.3	1

5.1. Constant strain rate tests

To evaluate the model's ability to capture the rate dependency of clays, we conducted a series of undrained triaxial compression and extension simulations on HKMD at various constant axial strain rates. For normally consolidated clays (OCR = 1), each sample was first isotropically consolidated at an initial confining pressure of 400 kPa. Then, the samples were sheared with three axial strain rates, i.e., 0.15, 1.5, and 15%/h, under both compression and extension states. For overconsolidated clays with OCRs = 2, 4, and 8, the preconsolidation pressures (p_c) were 200, 400, and 800 kPa, respectively. These samples were isotropically consolidated at a confining pressure of 100 kPa, then sheared at an axial strain rate of 1.5%/h.

Fig. 11 presents the measured and predicted results for normally consolidated clays. The results show that the model can capture the shear strength and stiffness response of HKMD under triaxial compression conditions at different axial strain rates. Note that in the triaxial extension simulations, the parameter n is set to 2.4 for a better prediction of shear strength. It can be seen that in the case of $D = 0.15$%/h, the predicted stress paths (Fig. 11(b)) for both compression and extension states will first shift somewhat to the left before moving upwards, rather than initially being perpendicular to the p-axis as observed in the cases of $D = 1.5$ and 15%/h. This is due to the fact that when the strain rate is extremely low, the clay is in a quasi-static state at the beginning of loading, resulting in very little change in the deviatoric stress. Overall, the predicted results are in good agreement with the experimental observations

for undrained triaxial tests at various strain rates.

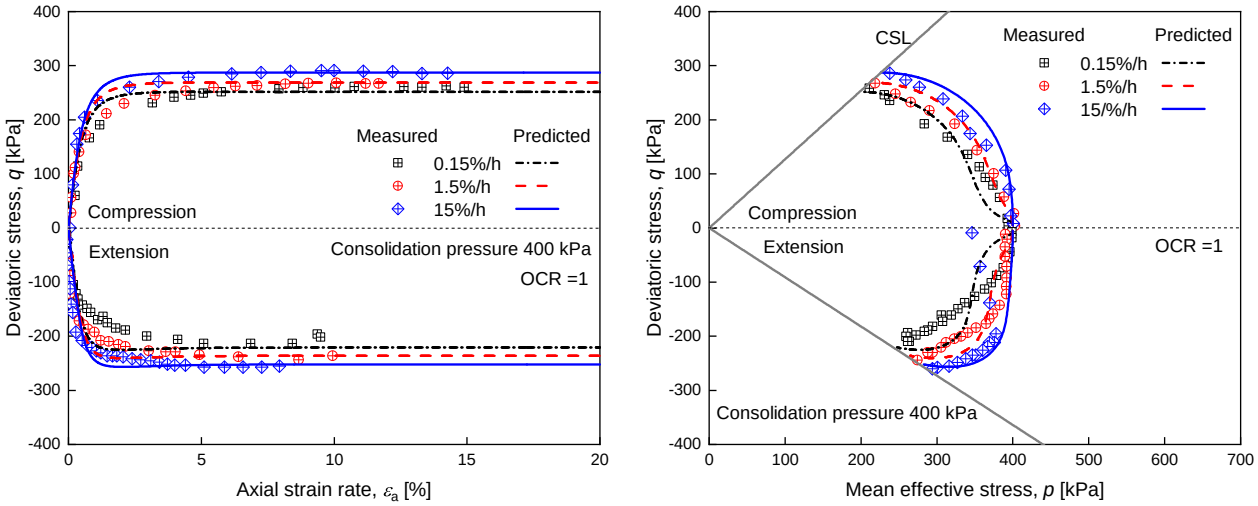

Figure 11: Comparison between experimental and numerical undrained triaxial tests on normally consolidated HKMD with different axial strain rates: (a) stress-strain curves; (b) stress paths.

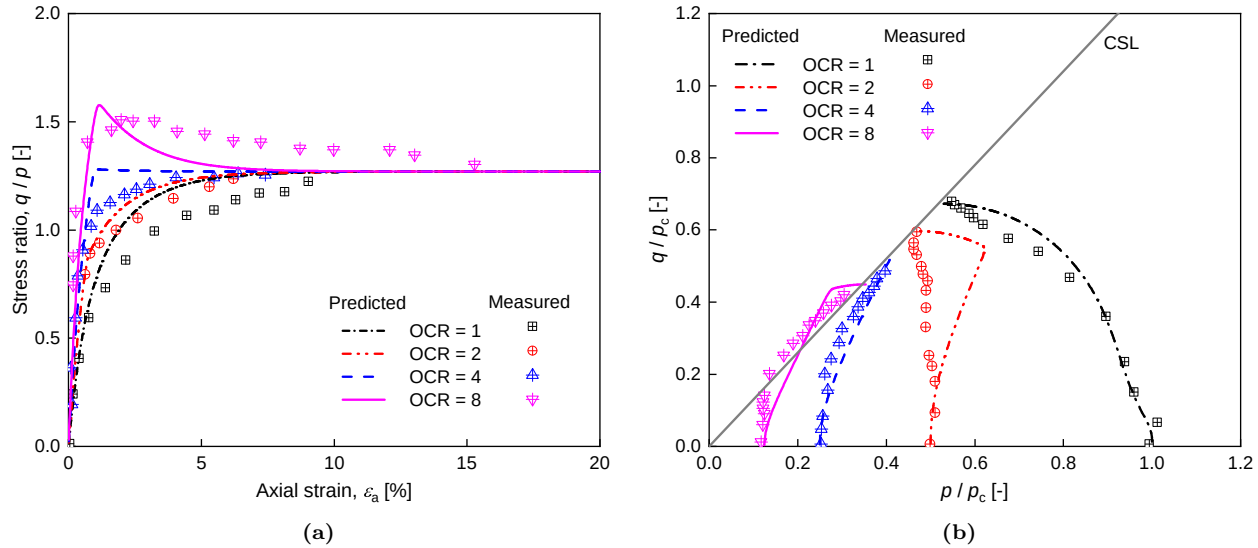

Figure 12: Comparison between experimental and numerical undrained triaxial tests on overconsolidated HKMD: (a) stress-strain curves; (b) stress paths.

Fig. 12 compares the measured and predicted results for clays with various OCRs at the same constant axial strain rate of 1.5%/h. Since the confining pressure applied on the overconsolidated clays is different from that applied on the normally consolidated clays, the measured and predicted stress paths were normalized with respect to the preconsolidation pressure p_c.

Overall, the stress-strain relationship and stress paths of overconsolidated clays at a constant strain rate can be reasonably predicted by the proposed model, although some discrepancies are observed in the stress path for clays with OCR = 2.

5.2. Stage-changed strain rate tests

In this section, undrained triaxial compression and oedometer tests with stage-changed axial strain rates on St. Herblain clay (Yin et al., 2010) were used for model validation. For triaxial tests, the clay samples were first anisotropically consolidated with a stress ratio of $k_0 = 0.9$, followed by a four-stage undrained shearing at constant strain rates varying from 0.1%-10%/h. The oedometer tests were performed at two different constant strain rates, i.e., loaded at $D = 3.3 \times 10^{-6}\text{s}^{-1}$ until a volumetric strain of 12%, then changed to $D = 6.6 \times 10^{-7}\text{s}^{-1}$, and finally returned to the initial axial strain rate.

Fig. 13(a) shows measured and predicted stress-strain relationships of undrained triaxial compression tests with stage-changed strain rates. The deviatoric stress changes with varying strain rates in experimental tests, which can be successfully captured by the proposed model. In simulations, the model predicts a rapid drop in stress when the axial strain rate significantly changes from 10 to 0.1%/h, e.g., at the onset of loading in the fourth stage in Fig. 13(a). This observation indicates that the model has the potential to simulate the stress relaxation of clays. Fig. 13(b) illustrates a comparison between model predictions and experimental results of oedometer tests. Overall, the comparison shows that the model can reasonably predict the oedometer compression of clays with stage-changed strain rates, although the horizontal stress under the same void ratio is slightly overestimated. Furthermore, this set of simulations demonstrates that the model is capable of describing the rate dependency of soft clays in both triaxial compression and oedometer states using a single set of model parameters, as discussed

in Section 4.2.

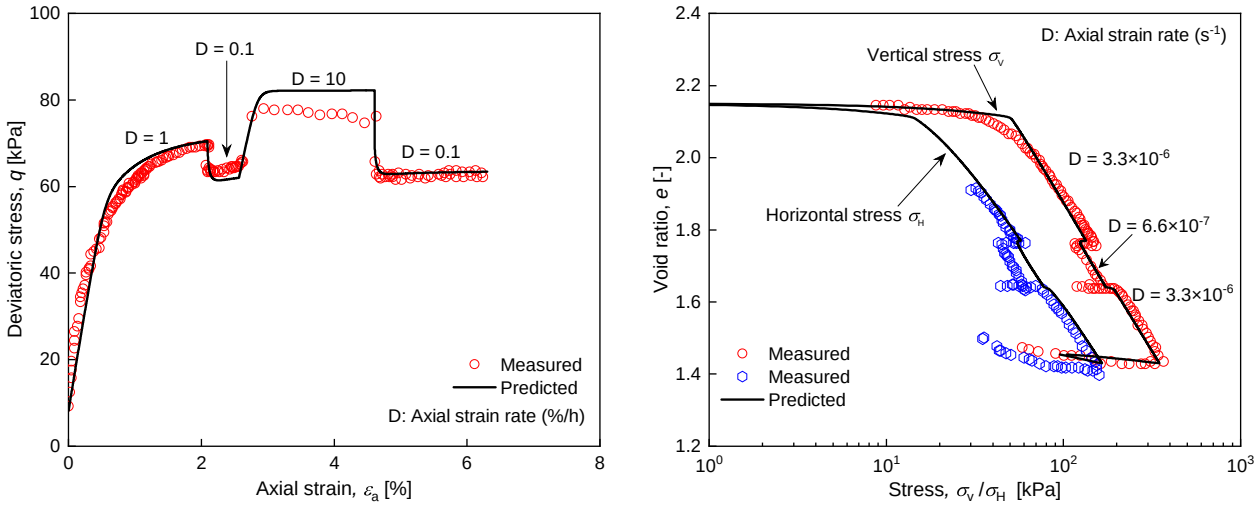

Figure 13: Comparison between experimental and numerical stage-changed strain rate tests on St. Herblain clay: (a) undrained triaxial compression test; (b) oedometer test.

5.3. Stress relaxation tests

We further conducted single- and multi-staged triaxial relaxation simulations to evaluate the model's predictive ability for the stress relaxation behaviour of clays. For single-staged relaxation simulations, the experimental results on HKMD from Zhu (2000) were used for validation.

Table 3: Numerical test scheduling for triaxial stress relaxation

Test No.	T_c/kPa	ε_a/%	D/%/h	OCR
CUC1	200	7.3	0.06	1
CUC2	400	17.1	1.5	1
CUE1	400	-9.5	-0.15	1
CUE2	200	-10.7	-1.5	1

Note: CUC (CUE) means consolidated undrained compression (extension) test.

In these simulations, clay samples were first sheared at constant strain rates until reaching a target axial strain. Then, the axial strain remains constant to investigate the variation of stress. Table 3 describes the test conditions in numerical simulations, where T_c means the initial

confining pressure, ε_a is the axial strain at the onset of stress relaxation, and D denotes the axial strain rate before stress relaxation starts.

Fig. 14 illustrates the evolution of the normalized deviatoric stress over time during tress relaxation, where q_0 denotes the deviatoric stress at the beginning of stress relaxation. The comparison between model predictions and experimental results indicates that the proposed model can effectively predict the stress relaxation of clays in single-staged tests under triaxial compression conditions. However, the predictions under triaxial extension conditions are not very satisfactory. The reason can be attributed to the fact that the developed model predicts the same initial stiffness under both triaxial compression and extension tests. Clay typically exhibits a lower initial stiffness under triaxial extension conditions compared to compression conditions (Sorensen et al., 2010). Consequently, at an identical axial strain rate, a slower stress decay rate can be observed during a single-staged relaxation test under triaxial extension conditions, resulting in higher deviatoric stress, as evidenced by samples CUC2 and CUE2 in Fig. 14. Although the developed model can predict varying strengths under triaxial compression and extension conditions, it fails to differentiate the predicted initial stiffnesses, as shown in Fig. 5. Therefore, a more pronounced difference can be observed between experiments and simulations under triaxial extension conditions. In addition, Both experiments and simulations suggest that the decay rate of deviatoric stress is primarily influenced by the initial axial strain rate applied to the clay. Specifically, a faster initial strain rate induces a more rapid decay rate of stress. Furthermore, many studies (Oda and Toshiyuki, 1988; Bagheri et al., 2019) have demonstrated that the relationship between the deviatoric stress and elapsed time during stress relaxation is almost linear in a semi-logarithmic coordinate system. Some interested readers can refer to Zhu (2000) for more details.

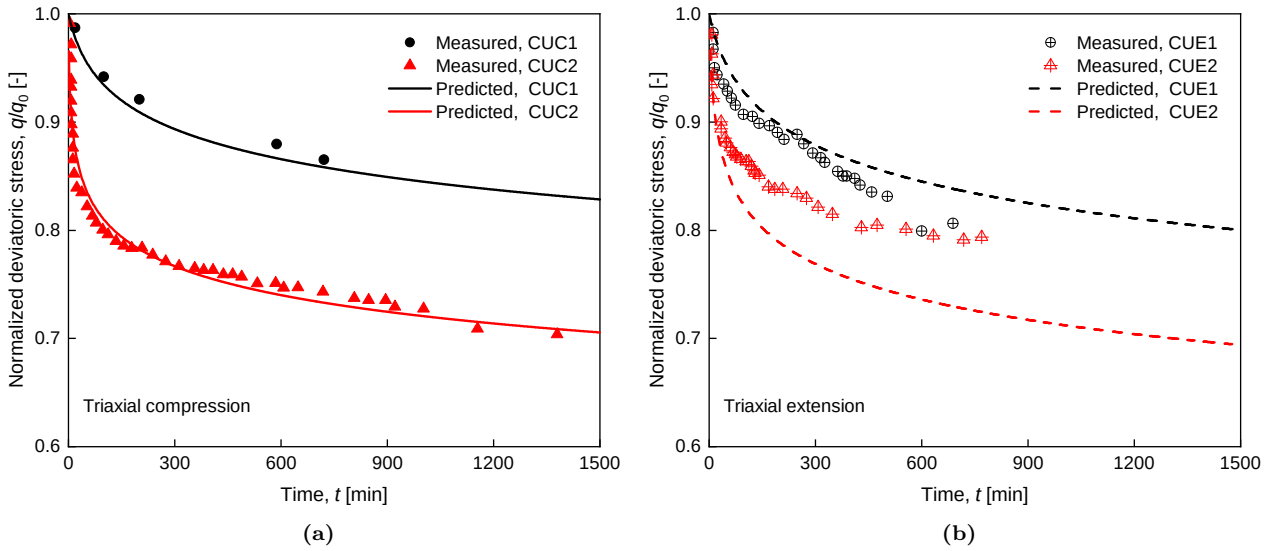

Figure 14: Comparison between experimental and numerical single-staged relaxation tests on HKMD: (a) triaxial compression test; (b) triaxial extension test.

Multi-staged stress relaxation tests on soft estuarine clay with different OCRs conducted by Kelln et al. (2008) were simulated for validation. During the tests, clay samples were first isotropically compressed to a confining pressure of 800 kPa, followed by an unloading stage until a confining pressure of 100 kPa. Those samples were then reloaded to confining pressures of 800 and 600 kPa to prepare normally consolidated (OCR = 1) and lightly overconsolidated (OCR = 1.33) clays. The shearing processes were divided into nine stages for normally consolidated samples and six for overconsolidated samples. Specifically, the sample was first sheared to a specific axial strain and then maintained at this strain to start the first-stage relaxation. After a period of stress relaxation, the sample was reloaded with a different axial strain, which was kept constant until the second-stage stress relaxation began, and so forth.

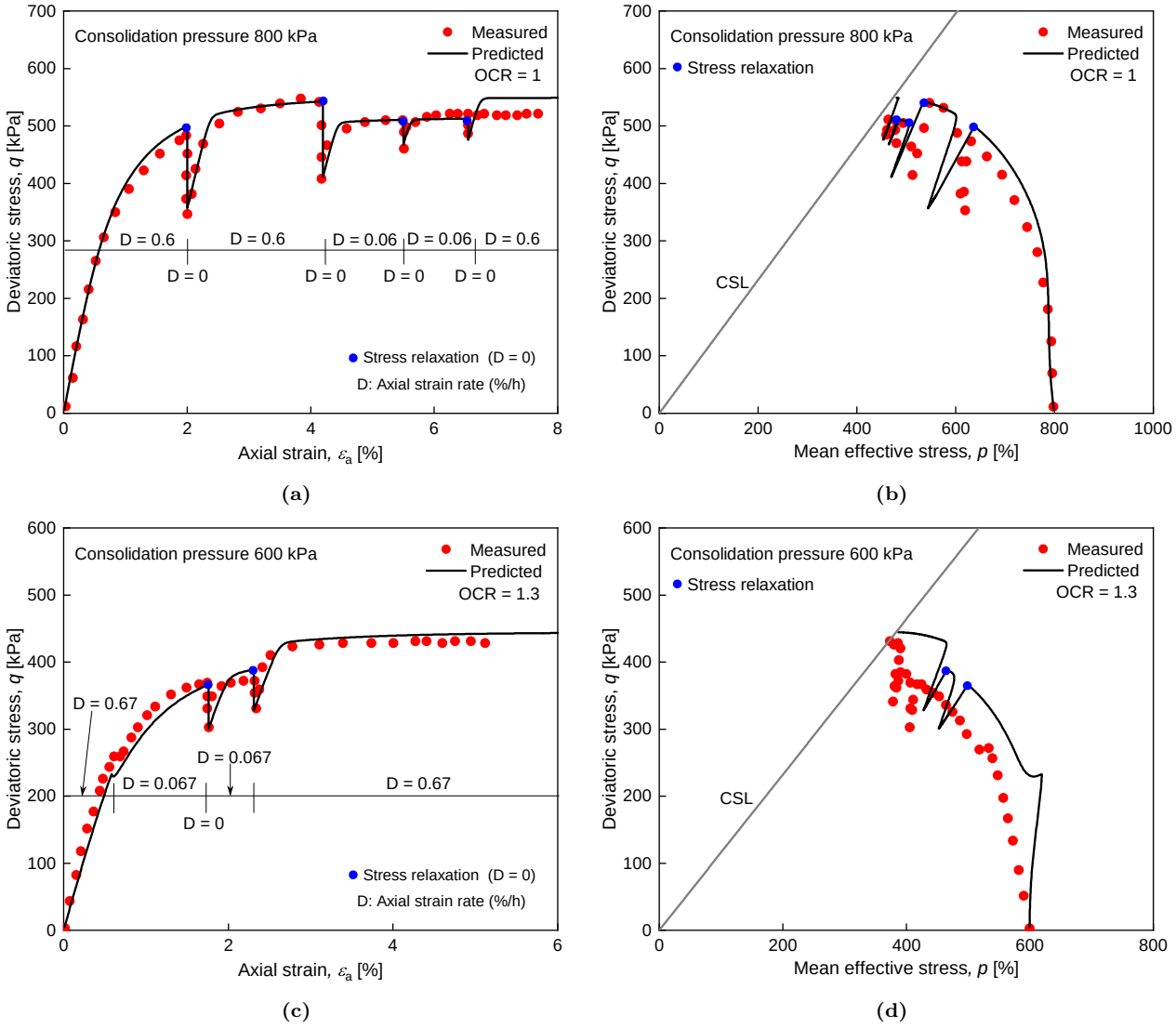

Figure 15: Comparison between experimental and numerical multi-staged relaxation tests on soft estuarine clay: (a) – (b) OCR = 1; (c) – (d) OCR = 1.3.

Fig. 15 presents the measured and predicted results, in which the blue marked points represent the phase transition points between the constant strain rate shearing and stress relaxation. It can be seen that the proposed model successfully captures the stress-strain curves for both normally consolidated and overconsolidated clays during stress relaxation. Nevertheless, there are some deviations between the predicted and measured stress paths. In Fig. 15(b), the measured deviatoric stress decreases at the first stress relaxation point while the mean effective stress remains constant. However, the predicted results show that both the deviatoric and

mean effective stresses decrease as they should. The same predictive results can be found in the literature (Yao et al., 2015). After the first relaxation stage, there is good agreement between the predicted and measured results. In Fig. 15(d), the predicted stress path exhibits a slight rightward shift compared to the experimental data. This difference can be attributed to the fast initial strain rate (0.6%/h in this case) applied to the sample at the onset of loading and the oveconsolidation effect, leading to a rapid decrease in the nonlinear term of the hypoplastic model. As a result, the predicted stress path will shift slightly to the right. This behaviour can also be observed in the hypoplastic models proposed by Niemunis (2003) and Yang et al. (2020).

5.4. Undrained creep tests

We finally evaluate the model's ability to predict the creep behaviour of soft clays. A series of undrained creep tests on HKMD conducted by Zhu (2000) were used for model validation. During the test, the soil samples were first isotropically and normally consolidated at a confining pressure of 400 kPa, then were instantly applied deviatoric stresses of 134, 289, and 234 kPa.

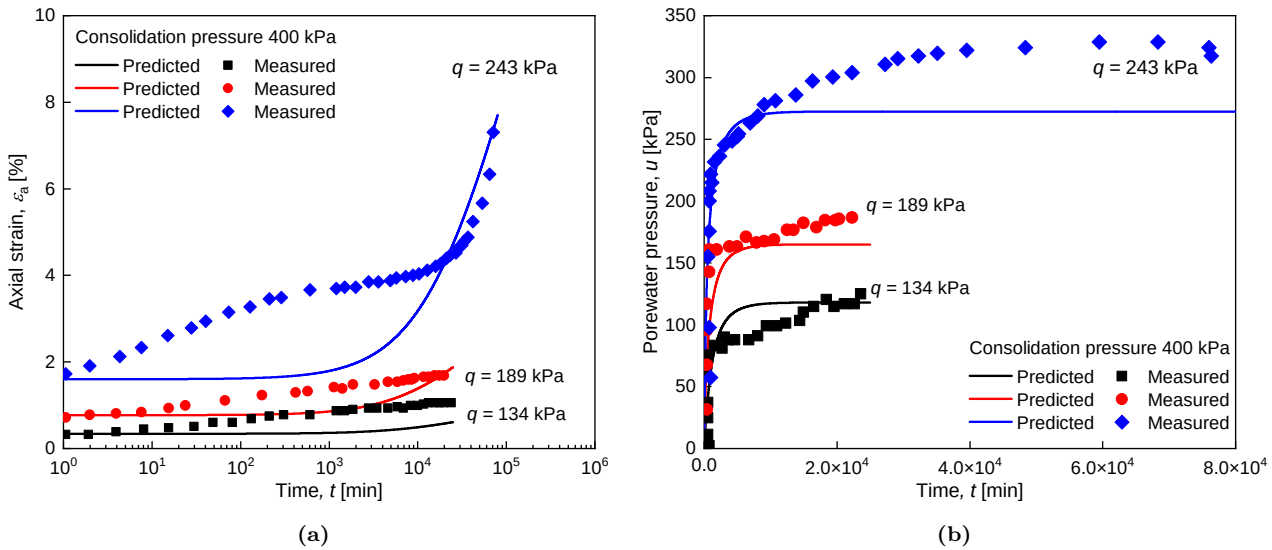

Figure 16: Comparison between experimental and numerical undrained creep tests on HKMD: (a) axial strain-time curves; (b) porewater pressure-time curves.

Fig. 16(a) illustrates the evolution of axial strain with elapsed time during the creep process. Notably, the model captures the accelerating creep characteristic of HKMD at higher stress levels, where axial strain rapidly increases with the elapsed time. Fig. 16(b) compares the measured and predicted effective porewater pressure developments during creep. The result shows that the model can predict the evolution of porewater pressure over time at lower stress levels while overestimating the porewater pressure at a higher stress level (243 kPa in this case).

6. Conclusions

In this paper, we proposed a visco-hypoplastic model to predict the stress-strain-time relationship of normally consolidated and overconsolidated clays under various loading conditions. The primary advantages and limitations of the proposed model are summarized as follows:

(1) The time-dependent behaviour of clays is considered in hypoplasticity by introducing a novel viscous strain rate derived from the isotach concept. This new viscous strain rate is then incorporated into the total strain rate of the hypoplastic framework, allowing viscous deformation at any stress state and enabling the stress rate to vary with the actual time increment. Furthermore, this viscous flow is directly linked to the overconsolidation ratio, providing a reasonable description of the time effect on both normally consolidated and overconsolidated clays.

(2) The viscous strain rate formulated in this paper resembles that proposed by Niemunis (2003) but with enhanced physical significance. The latter is established analogously to Norton's power law, where a reference creep rate is used with its value empirically given rather than experimentally determined. The newly derived viscous strain rate is mathematically formulated, with all parameters having explicit physical meanings and obtainable through laboratory tests.

(3) The linear and nonlinear terms of the proposed model stem from the four-parameter

hypoplastic model proposed by Wu et al. (2017). Therefore, the conical failure surface from this model is preserved in the proposed model, ensuring consistent shear strength predictions across triaxial compression and tension tests. In this paper, the transformed stress technique is used to incorporate the Matsuoka-Nakai failure criterion into the proposed model. As a result, the stress-strain-time relationship of clays under multiaxial conditions can be predicted by the proposed model.

(4) The initial stiffness of the proposed model remains constant when predicting overconsolidated clays, which conflicts with the experimental observation that the initial stiffness increases with increasing the overconsolidation ratio (OCR). This limitation is addressed by introducing a new scalar stiffness function into the proposed model. This function can reproduce the variation in initial stiffness for clays when OCR changes without affecting the peak strength and critical state.

(5) Natural soft clays usually possess internal structures and inherent anisotropy. However, these features are not considered in the proposed model. As a result, the proposed model cannot predict the time-dependent behaviour of clays related to structural degradation and strength anisotropy.

CRediT authorship contribution statement

Yu-Qi He: Conceptualization, Data Curation, Formal Analysis, Investigation, Methodology, Writing – Original Draft Preparation.

Zhen-Yu Yin: Conceptualization, Funding Acquisition, Methodology, Project Administration, Resources, Supervision, Writing – Review & Editing.

Shun Wang: Investigation, Methodology, Writing – Review & Editing.

Declaration of Competing Interest

The authors declare that they have no known competing financial interests or personal relationships that could have appeared to influence the work reported in this paper.

Data availability statement

All data that support the findings of this study are available from the corresponding author upon reasonable request.

Acknowledgements

This research is financially supported by the Research Grants Council (RGC) of Hong Kong Special Administrative Region Government (HKSARG) of China (Grant Nos.: 15217220; N_PolyU534/20) and the National Natural Science Foundation of China (Grant No.: 42472355).

Appendix A.

The proposed visco-hypoplastic model is formulated as

$$\mathring{\mathbf{T}} = f_s \boldsymbol{\mathcal{L}} : (\mathbf{D} - \mathbf{D}_{vis}^{new}) \tag{A.1}$$

where $\mathbf{D}_{vis}^{new}$ means the new viscous strain rate tensor:

$$\mathbf{D}_{vis}^{new} = \beta \frac{R^{\alpha}}{t_0} \mathbf{B} \tag{A.2}$$

in which $\alpha = (\lambda^* - \kappa^*)/\beta$ and $R = 1/\mathrm{OCR}$. $\mathbf{B}$ denotes the flow rule of the hypoplastic model:

$$\mathbf{B} = \frac{\mathbf{D}}{\|\mathbf{D}\|} = -\boldsymbol{\mathcal{L}}^{-1} : \mathbf{N} \tag{A.3}$$

in which the fourth-order tensor $\boldsymbol{\mathcal{L}}$ and the second-order tensors $\mathbf{N}$ are expressed as

$$\boldsymbol{\mathcal{L}} = (\mathrm{tr}\mathbf{T})\boldsymbol{\mathcal{I}} + f_v\mathbf{T}\otimes\mathbf{I} + a^2\frac{\mathbf{T}\otimes\mathbf{T}}{\mathrm{tr}\mathbf{T}} \tag{A.4a}$$

$$\mathbf{N} = f_u a(\mathbf{T}+\mathbf{T}^*) \tag{A.4b}$$

The functions f_s, f_v, and f_u are defined as

$$f_s = -\frac{2\delta_s}{3v_i\lambda^*}, \qquad f_v = \frac{3}{2}v_i - \frac{1}{3}(3+a^2-\sqrt{3}a), \qquad f_u = \frac{|\mathbf{B}:\mathbf{D}|}{\|\mathbf{B}\|\,\|\mathbf{D}\|} \tag{A.5}$$

in which δ_s is a stiffness multiplier:

$$\delta_s = \frac{\exp[\zeta\ln(\mathrm{OCR})]}{(1+r_s^2)} \tag{A.6}$$

where ζ is a material parameter controlling the initial stiffness of the overconsolidated sample. The stress ratio $r_s = \|\mathbf{T}^*\|/\mathrm{tr}\mathbf{T}$.

The strength parameter a is expressed as

$$a = \frac{\sqrt{3}(3-\sin\varphi)}{2\sqrt{2}\varphi} \tag{A.7}$$

where φ is the critical friction angle.

The overconsolidation ratio OCR is defined as

$$\mathrm{OCR} = p_e/p_e^+ \tag{A.8}$$

with

$$p_e = \exp\Big[\frac{N-\ln(1+e)}{\lambda^*}\Big], \quad p_e^+ = p\Big[1+\frac{1}{n}\big(\frac{q}{Mp}\big)^{(n+1)}\Big] \tag{A.9}$$

There are nine parameters for the proposed model, including five basic parameters: N, λ^*, κ^*, v_i, and φ, two viscous parameters: β and t_0, and two additional parameters: ζ and n.

Appendix B.

The expressions of several generally used failure criteria in the transformed stress method are given subsequently. According to Tian and Yao (2017), A mapping from the original stress tensor $\mathbf{T}$ to the transformed stress tensor $\widetilde{\mathbf{T}}$ can be written as follows:

$$\widetilde{\mathbf{T}} = \begin{cases} \dfrac{\mathrm{tr}\mathbf{T}}{3}\mathbf{I} + \dfrac{q_c}{q}\mathbf{T}^*, & (q \neq 0) \\ \mathbf{T}, & (q = 0) \end{cases} \tag{B.1}$$

where q is the deviatoric stress, and q_c means the deviatoric stress under the triaxial compression condition on the π-plane.

Based on the Matsuoka-Nakai (SMP) criterion (Matsuoka et al., 1999), q_c can be expressed as

$$q_c = \frac{2I_1}{3\sqrt{(I_1I_2 - I_3)/(I_1I_2 - 9I_3)} - 1} \tag{B.2}$$

Based on Lade's criterion (Yao and Sun, 2000), q_c can be expressed as

$$q_c = I_1\left(1 - \frac{1}{2}\sqrt{\frac{9I_3}{{I_1}^3}}\left\{\cos\left[\frac{1}{3}\cos^{-1}\left(-\sqrt{\frac{9I_3}{{I_1}^3}}\right)\right]\right\}^{-1}\right) \tag{B.3}$$

Based on the unified failure criterion (Yao et al., 2004), q_c can be expressed as

$$q_c = \omega\sqrt{{I_1}^2 - 3I_2} + \frac{2(1-\omega)I_1}{3\sqrt{(I_1I_2 - I_3)/(I_1I_2 - 9I_3)} - 1} \tag{B.4}$$

in which I_1, I_2, and I_3 are stress invariants.:

$$I_1 = \mathrm{tr}\mathbf{T}, \quad I_2 = 0.5[\mathbf{T}{:}\mathbf{T} - (I_1)^2], \quad I_3 = \det\mathbf{T} \tag{B.5}$$

where $\det\mathbf{T}$ means the determinant of $\mathbf{T}$. ω is a weighting factor ranging from 0 to 1.

As shown in Fig. B.17, when $\omega = 0$, the failure curve on the π-plane is a circle, corresponding to the Drucker-Prager (DP) failure criterion (Drucker and Prager, 1952); when $\omega = 1$, the failure curve on the π-plane is a curved triangle, corresponding to the SMP criterion; when $0 < \omega < 1$, the failure curve on the π-plane changes smoothly from the DP criterion to the SMP criterion.

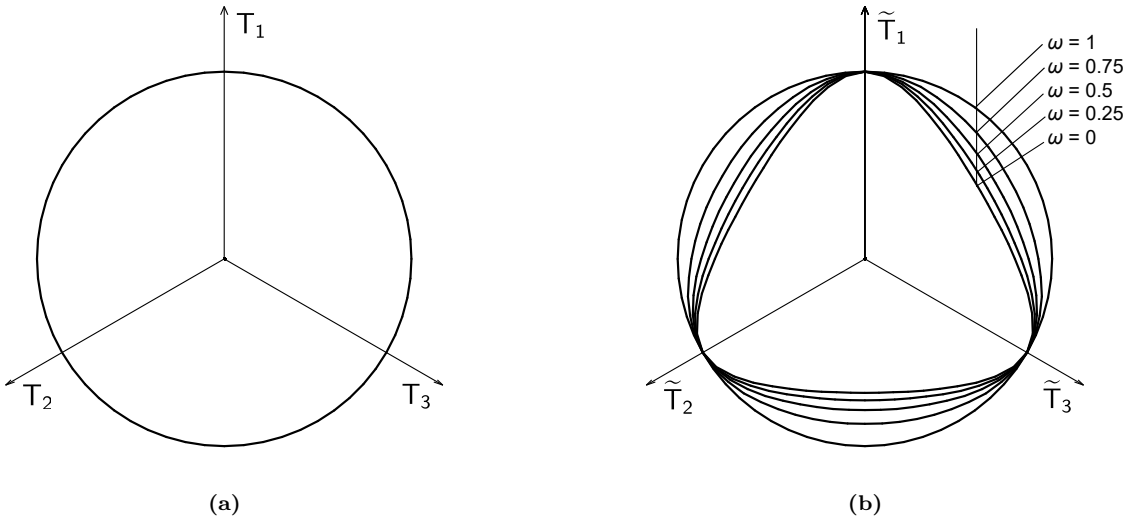

Figure B.17: Failure surfaces of the hypoplastic model: (a) original; (b) after transformation.

References

Acikel, A.S., Gates, W.P., Singh, R.M., Bouazza, A., Fredlund, D.G., Rowe, R.K., 2018. Time-dependent unsaturated behaviour of geosynthetic clay liners. Can. Geotech. J. 55 (12), 1824–1836.

Adachi, T., Oka, F., 1982. Constitutive equations for normally consolidated clay based on elasto-viscoplasticity. Soils Found. 22 (4), 57–70.

554 Bagheri, M., Rezania, M., Mousavi Nezhad, M., 2019. Rate dependency and stress relaxation
555 of unsaturated clays. Int. J. Geomech. 19 (12), 04019128.

556 Bjerrum, L., 1967. Engineering geology of Norwegian normally-consolidated marine clays as
557 related to settlements of buildings. Géotechnique 17 (2), 83–118.

558 Cheng, W., Yin, Z.Y., 2024. Fractional order viscoplastic modeling of anisotropically overcon-
559 solidated clays with modified isotach viscosity. Int. J. Plast. 172, 103858.

560 Drucker, D.C., Prager, W., 1952. Soil mechanics and plastic analysis or limit design. Q. Appl.
561 Math. 10 (2), 157–165.

562 Freitas, T.M.B., Potts, D.M., Zdravkovic, L., 2011. A time dependent constitutive model for
563 soils with isotach viscosity. Comput. Geotech. 38 (6), 809–820.

564 Fuentes, W., Lizcano, A., 2010. Visco-hypoplastic model for structured soils. GeoFlorida 2010:
565 Advances in Analysis, Modeling & Design, pp. 452–460.

566 Fuentes, W., Tafili, M., Triantafyllidis, T., 2018. An ISA-plasticity-based model for viscous and
567 non-viscous clays. Acta Geotech. 13, 367–386.

568 Gudehus, G., 2004. A visco-hypoplastic constitutive relation for soft soils. Soils Found. 44
569 (4), 11–25.

570 Han, J., Yin, Z.Y., Dano, C., Hicher, P.Y., 2021. Cyclic and creep combination effects on the
571 long-term undrained behavior of overconsolidated clay. Acta Geotech. 16, 1027–1041.

572 He, Y.Q., Liao, H.J., Wu, W., Wang, S., 2023. Hypoplastic modeling of inherent anisotropy in
573 normally and overconsolidated clays. Acta Geotech. 18 (12), 6315–6333.

He, Y.Q., Wang, S., Liao, H.J., Wu, W., 2022. A hypoplastic constitutive model for structured soils. Comput. Geotech. 151, 104935.

Jerman, J., Mašín, D., 2020. Hypoplastic and viscohypoplastic models for soft clays with strength anisotropy. Int. J. Numer. Anal. Methods Geomech. 44 (10), 1396–1416.

Karim, M.R., Gnanendran, C.T., 2014. Review of constitutive models for describing the time dependent behaviour of soft clays. Geomech. Geoeng. 9 (1), 36–51.

Karstunen, M., Yin, Z.Y., 2010. Modelling time-dependent behaviour of Murro test embankment. Géotechnique 60 (10), 735–749.

Kelln, C., Sharma, J., Hughes, D., Graham, J., 2008. An improved elastic–viscoplastic soil model. Can. Geotech. J. 45 (10), 1356–1376.

Kutter, B.L., Sathialingam, N., 1992. Elastic-viscoplastic modelling of the rate-dependent behaviour of clays. Géotechnique 42 (3), 427–441.

Lai, X.L., Wang, S.M., Ye, W.M., Cui, Y.J., 2014. Experimental investigation on the creep behavior of an unsaturated clay. Can. Geotech. J. 51 (6), 621–628.

Leroueil, S., Kabbaj, M., Tavenas, F., Bouchard, R., 1985. Stress–strain–strain rate relation for the compressibility of sensitive natural clays. Géotechnique 35 (2), 159–180.

Liang, J., Lu, D., Zhou, X., Du, X., Wu, W., 2019. Non-orthogonal elastoplastic constitutive model with the critical state for clay. Comput. Geotech. 116, 103200.

Liang, J., Ma, C., Su, Y., Lu, D., Du, X., 2022. A failure criterion incorporating the effect of depositional angle for transversely isotropic soils. Comput. Geotech. 148, 104812.

Liao, D., Hu, X.J., Wang, S., Zhou, C., 2024. Improvement of a hypoplastic model for sand under undrained loading conditions. Can. Geotech. J. (ja).

Liao, D., Yang, Z.X., 2021. Hypoplastic modeling of anisotropic sand behavior accounting for fabric evolution under monotonic and cyclic loading. Acta Geotech. 16, 2003–2029.

Lu, D., Liang, J., Du, X., Ma, C., Gao, Z., 2019. Fractional elastoplastic constitutive model for soils based on a novel 3D fractional plastic flow rule. Comput. Geotech. 105, 277–290.

Lu, D., Ma, C., Du, X., Jin, L., Gong, Q., 2017. Development of a new nonlinear unified strength theory for geomaterials based on the characteristic stress concept. Int. J. Geomech. 17 (2), 04016058.

Mašín, D., 2005. A hypoplastic constitutive model for clays. Int. J. Numer. Anal. Methods Geomech. 29 (4), 311–336.

Mašín, D., 2007. A hypoplastic constitutive model for clays with meta-stable structure. Can. Geotech. J. 44 (3), 363–375.

Matsuoka, H., 1974. Stress-strain relationships of sands based on the mobilized plane. Soils Found. 14 (2), 47–61.

Matsuoka, H., Yao, Y.P., Sun, D.A., 1999. The Cam-clay models revised by the SMP criterion. Soils Found. 39 (1), 81–95.

Niemunis, A., 2003. Extended hypoplastic models for soils. Vienna: Inst. für Grundbau und Bodenmechanik.

Niemunis, A., Grandas-Tavera, C.E., Prada-Sarmiento, L.F., 2009. Anisotropic visco-hypoplasticity. Acta Geotech. 4, 293–314.

615 Oda, Y., Toshiyuki, M., 1988. Stress relaxation characteristics of saturated clays. Soils Found. 28
616 (4), 69–80.

617 Perzyna, P., 1963. The constitutive equations for rate sensitive plastic materials. Q. Appl.
618 Math. 20 (4), 321–332.

619 Qian, H.Y., Wu, W., Xu, C.S., Du, X.L., 2023. A hypoplastic model for hydrate-bearing
620 sand considering hydrate saturation and grain breakage. Int. J. Numer. Anal. Methods
621 Geomech. 47 (16), 3044–3064.

622 Qian, H.Y., Xu, C.S., Wu, W., Du, X.L., 2024. A hypoplastic model considering grain breakage
623 and wetting effect for granular material. Comput. Geotech. 171, 106329.

624 Sorensen, K.K., Baudet, B.A, Simpson, B., 2010. Influence of strain rate and acceleration on
625 the behaviour of reconstituted clays at small strains. Géotechnique 60 (10), 751–763.

626 Šuklje, L., 1957. The analysis of the consolidation process by the isotache method. In: Pro-
627 ceedings of the 4th International Conference on Soil Mechanics and Foundation Engineering.
628 London, 1, pp. 200–206.

629 Tian, Y., Yao, Y.P., 2017. A simple method to describe three-dimensional anisotropic failure
630 of soils. Comput. Geotech. 92, 210–219.

631 Wang, H., Cui, Y.J., 2024. A viscoplastic constitutive model for unsaturated soils based on
632 nonstationary flow surface theory. Int. J. Numer. Anal. Methods Geomech. 48 (2), 476–495.

633 Wang, H., Cui, Y.J., Vu, M.N., Talandier, J., 2024. Strain-rate effect on the hydro-mechanical
634 behaviour of unsaturated damaged Callovo–Oxfordian claystone. Acta Geotech. 19 (7), 4313–
635 4324.

636 Wang, S., Wu, W., 2021. Validation of a simple hypoplastic constitutive model for overconsol-
637 idated clays. Acta Geotech. 16, 31–41.

638 Wang, S., Wu, W., Yin, Z.Y., Peng, C., He, X.Z., 2018. Modelling the time-dependent be-
639 haviour of granular material with hypoplasticity. Int. J. Numer. Anal. Methods Geomech. 42
640 (12), 1331–1345.

641 Wang, Y.D., Wu, W.,2024. Numerical model for solid-like and fluid-like behavior of granular
642 flows. Acta Geotech. 1–12.

643 Wu, W., Bauer, E., 1994. A simple hypoplastic constitutive model for sand. Int. J. Numer.
644 Anal. Methods Geomech. 18 (12), 833–862.

645 Wu, W., Kolymbas, D., 2000. Hypoplasticity then and now. Constitutive Modelling of Granular
646 Materials. Springer, Berlin, Heidelberg, pp. 57–105.

647 Wu, W., Lin, J., Wang, X.T., 2017. A basic hypoplastic constitutive model for sand. Acta
648 Geotech. 12, 1373–1382.

649 Xu, G.F., Wu, W., Qi, J.L., 2016. Modeling the viscous behavior of frozen soil with hypoplas-
650 ticity. Int. J. Numer. Anal. Methods Geomech. 40 (15), 2061–2075.

651 Yang, C., Carter, J.P., Sheng, D.C., Sloan, S.W., 2016. An isotach elastoplastic constitutive
652 model for natural soft clays. Comput. Geotech. 77, 134–155.

653 Yang, Z.X., Liao, D., Xu, T.T., 2020. A hypoplastic model for granular soils incorporating
654 anisotropic critical state theory. Int. J. Numer. Anal. Methods Geomech. 44 (6), 723–748.

655 Yao, Y.P., Kong, L.M., Zhou, A.N., Yin, J.H., 2015. Time-dependent unified hardening

656 model: three-dimensional elastoviscoplastic constitutive model for clays. J. Eng. Mech. 141
657 (6), 04014162.

658 Yao, Y.P., Lu, D.C., Zhou, A.N., Zou, B., 2004. Generalized non-linear strength theory and
659 transformed stress space. Sci. China Ser. E 47, 691–709.

660 Yao, Y.P., Sun, D.A., 2000. Application of Lade's criterion to Cam-clay model. J. Eng.
661 Mech. 126 (1), 112–119.

662 Yin, J.H., Graham, J., 1999. Elastic viscoplastic modelling of the time-dependent stress-strain
663 behaviour of soils. Can. Geotech. J. 36 (4), 736–745.

664 Yin, J.H., Zhu, J.G., Graham, J., 2002. A new elastic viscoplastic model for time-dependent
665 behaviour of normally and overconsolidated clays: theory and verification. Can. Geotech.
666 J. 39 (1), 157–173.

667 Yin, Z.Y., Chang, C.S., Karstunen, M., Hicher, P.Y., 2010. An anisotropic elastic–viscoplastic
668 model for soft clays. Int. J. Solids Struct. 47 (5), 665–677.

669 Yin, Z.Y., Jin, Y.F., Shen, S.L., Huang, H.W., 2017. An efficient optimization method for
670 identifying parameters of soft structured clay by an enhanced genetic algorithm and elastic–
671 viscoplastic model. Acta Geotech. 12, 849–867.

672 Yin, Z.Y., Karstunen, M., Chang, C.S., Koskinen, M., Lojander, M., 2011. Modeling time-
673 dependent behavior of soft sensitive clay. J. Geotech. Geoenviron. Eng. 137 (11), 1103–1113.

674 Yin, Z.Y., Yin, J.H., Huang, H.W., 2015. Rate-dependent and long-term yield stress and
675 strength of soft Wenzhou marine clay: experiments and modeling. Mar. Georesources
676 Geotechnol. 33 (1), 79–91.

Yuan, Y.X., Whittle, A.J., 2021. Formulation of a new elastoviscoplastic model for time-dependent behavior of clay. Int. J. Numer. Anal. Methods Geomech. 45 (6), 843–864.

Zhang, W., Wang, S., Wu, Y., Wu, W., 2021. Bifurcation analysis of shear band in sand under true triaxial conditions with hypoplasticity. Int. J. Numer. Anal. Methods Geomech. 45 (7), 934–949.

Zhao, R., Zhou, A., Yao, Y.P., 2024. The UTUH model: a time-dependent unified hardening constitutive model for unsaturated soils. Acta Geotech. 19 (4), 1649–1666.

Zhu, C.W., Wu, W., Peng, C., Wang, S., Wei, X., 2024. SPH implementation of a critical state-based hypoplastic model for granular materials in large-deformation problems. Comput. Geotech. 166, 106011.

Zhu, J.G., 2000. Experimental study and elastic visco-plastic modelling of the time-dependent stress-strain behaviour of Hong Kong marine deposits. (Ph.D. thesis). Hong Kong Polytechnic University.